Subthermocline Countercurrents in the Western Equatorial Atlantic Ocean

JOHN D. COCHRANE, FRANCIS J. KELLY, JR., AND CHARLES R. OLLING

Department of Oceanography, Texas A&M University, College Station 77843

(Manuscript received 25 October 1978, in final form 16 January 1978)

ABSTRACT

In each hemisphere of the Atlantic, a permanent countercurrent (eastward flow) having a core about 4.5° from the Equator is present in the subthermocline layer from 80 to 200 cl t^{-1} (centiliters per metric ton). Although currents along the Brazilian coast supply water to the countercurrents, much of the flow in each seems to be internal to the anticyclonic region on its equatorward side. West of 25°W, the region considered here, the south countercurrent is covered largely by westward flow, has a mean width of 209 km, and a mean geostrophic transport of 15×10^6 m^3 s^{-1}. The north countercurrent often lies below eastward flow, but its core is marked by a subthermocline velocity maximum and a path differing from that of the navifacial core. Between about 50 and 40°W, available data indicate a mean transport of 9×10^6 m^3 s^{-1} in February–April and 26×10^6 m^3 s^{-1} in July–September, a significant annual variation. From 40 to 28°W, roughly, evidence for a permanent subthermocline countercurrent is strongest. The current has a mean uninterrupted width of 231 km. Its transport shows no significant annual variation and has a mean of 19×10^6 m^3 s^{-1}. East of about 28°W, the north countercurrent breaks up. The flux mode of the south, and the strong sector of the north, countercurrent is in the layer from 120 to 140 cl t^{-1}, the main part of the equatorial thermostad. Transports of the Atlantic subthermocline countercurrents are considerably larger than those reported for their Pacific counterparts.

1. Introduction

Geostrophic velocity computations reveal a strong countercurrent below the most intense part of the thermocline on either side of the equator in the Atlantic Ocean. The countercurrents are similar in situation and structure to the subsurface countercurrents in the Pacific Ocean which Tsuchiya (1972, 1975) has described. The presence of countercurrents in subthermocline depths of the equatorial Atlantic was noted by Cochrane (1965, 1968a, b). Reid (1964), Khanaychenko and Khlystov (1966), Mazeika (1968), Khanaychenko (1970) and others have commented on the existence of a South Equatorial Countercurrent in the Atlantic. Cochrane (1975) recognized that there is a subthermocline current core in the countercurrents of the Atlantic. Hisard *et al.* (1976) described the extent and permanence of the subsurface, i.e., subthermocline, countercurrents. The present paper investigates the subthermocline countercurrents in the equatorial Atlantic west of 25°W, providing descriptions of their velocity structures, transports and origins and examining evidence for their permanence.

The velocity v relative to its value v_0 at a reference pressure p_0 is obtained from the mass distribution by means of the geostrophic equations (vertically integrated thermal wind equations)

$$f(v - v_0) = \left[\frac{\partial(\phi - \phi_0)}{\partial l}\right]_p = \int_{\delta_0}^{\delta} \left(\frac{\partial p}{\partial l}\right)_\delta d\delta = \left[\frac{\partial(\Upsilon - \Upsilon_0)}{\partial l}\right]_\delta, \quad (1)$$

where f is the Coriolis parameter, ϕ the geopotential anomaly, p pressure, δ the steric anomaly, and Υ the acceleration potential (Montgomery, 1937; Montgomery and Spilhaus, 1941). The distance l is measured along some line, usually along a transect. The positive direction along the line is taken so that $v - v_0$, the component 90° clockwise from the direction, is positive when it has an eastward component. Essentially these equations are discussed by Montgomery and Wooster (1954). The first is the most familiar form. The second is useful in interpreting the slopes of steric (and, approximately, isanosteric) surfaces. The third permits computation of horizontal velocity at a steric anomaly surface. Acceleration potential is obtained from geopotential anomaly by changing the variable of integration from p to δ, i.e.,

$$\Upsilon - \Upsilon_0 = \phi - \phi_0 + p\delta = \int_{\delta_0}^{\delta} p d\delta + p_0\delta_0.$$

Water parcels tend to move along surfaces of constant potential steric anomaly because of vertical

0022-3670/79/040724-15$07.75

stabilizing forces (Montgomery, 1937, 1938; Reid, 1965; Tsuchiya, 1968; Reid and Lynn, 1971). These surfaces are closely approximated at shallower depths by surfaces of constant thermosteric anomaly, isanosteric surfaces (Montgomery and Wooster, 1954). For application to such surfaces, the third form of Eq. (1) must be modified. In accordance with Montgomery (1937), the appropriate form is

$$f(v - v_0) = \left[\frac{\partial(\Upsilon - \Upsilon_0)}{\partial l}\right]_{\delta_T} - p\left(\frac{\partial \delta_p}{\partial l}\right)_{\delta_T}, \quad (2)$$

where $\delta_p = \delta_{s,p} + \delta_{t,p} + \delta_{s,t,p}$ (Bjerknes and collaborators, 1910). The second term on the right is usually small at pressures <1000 db, as Montgomery (1938) noted. Thus a map of acceleration potential provides a good approximation of the velocity field at a thermosteric anomaly surface. However, the term often contributes significantly in computations of geostrophic volume transport in the equatorial Atlantic and is therefore retained in all velocity computations.

The subthermocline countercurrents are introduced by means of vertical sections of thermosteric anomaly. Their extent in the Atlantic west of 25°W is sketched in the distribution of acceleration potential on the surface, where δ_T = 140 cl t^{-1}, which lies somewhat below the strongest thermocline layers. Geostrophic velocities and transports in the layer from 80 to 200 cl t^{-1} provide an assessment of the strength and permanence of the currents.

2. Vertical structure

Figs. 1a and 1b show the vertical sections of the thermosteric anomaly for transects taken at 30°W in February 1963 and near 33°W in August 1963, respectively. The sections illustrate features which imply the presence of the subthermocline countercurrents. The isanostere of 100 cl t^{-1} in Fig. 1a and those of 100 and 120 cl t^{-1} in Fig. 1b have a W shape roughly symmetric about the Equator. The outer sides of the W between 3° and 7°, roughly, in either hemisphere represent, according to the second form of Eq. (1), regions where the eastward flow component increases with height. (The form is not clearly marked in the Northern Hemisphere of Fig. 1a.) In the south, the isanosteres become level

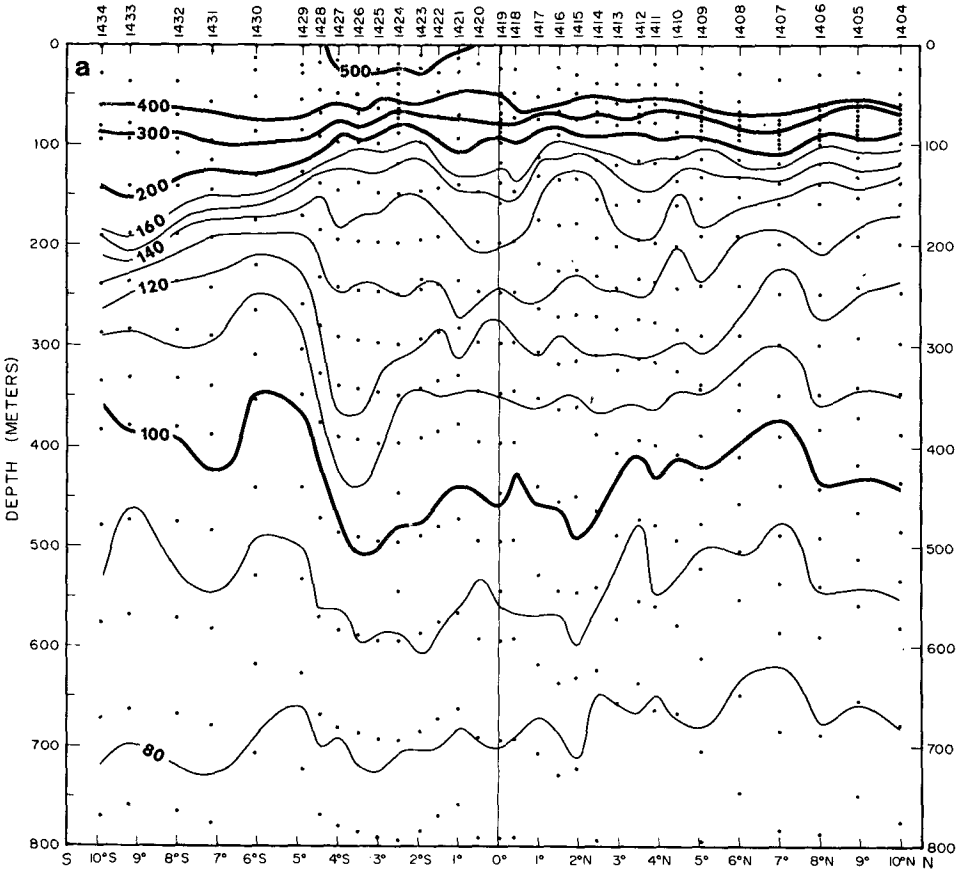

FIG. 1a. Vertical section of thermosteric anomaly (cl t^{-1}) along 30°W from the *Crawford* cruise of Equalant I (5–14 March 1963). Vertical exaggeration 2.76 × 10^3:1. Station positions are given at top. Location is shown in Fig. 2a.

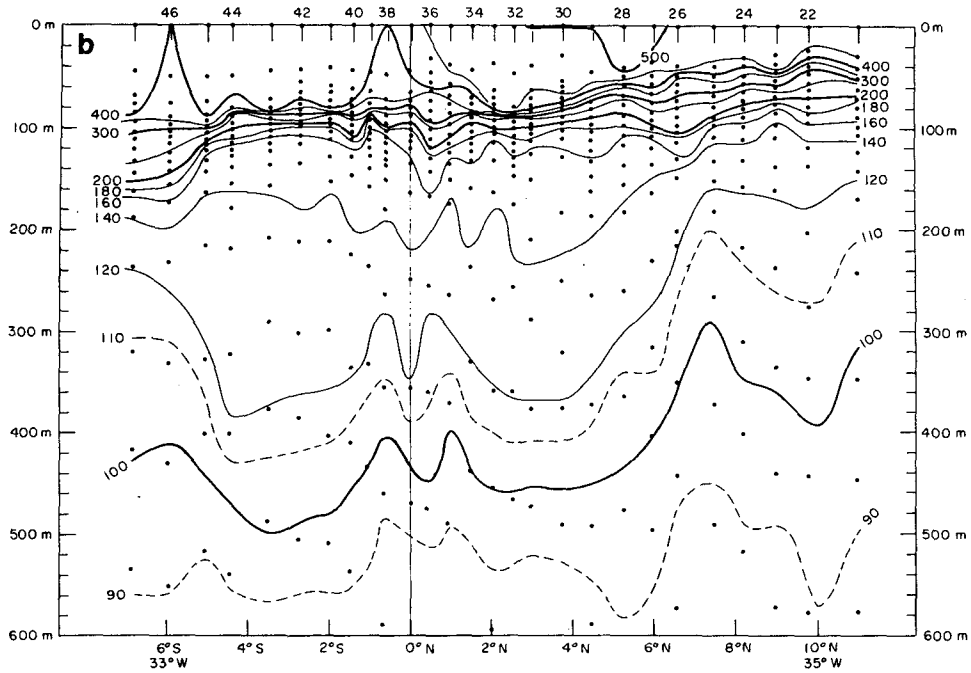

FIG. 1b. Vertical section of thermosteric anomaly (cl t^{-1}) near 33°W from the *Laserre* cruise of Equalant II (11–20 August 1963). Vertical exaggeration 2.76 × 10^3:1. Station positions are given at top. Location is shown in Fig. 4.

near 140 cl t^{-1} and reverse their slope above so that the relative eastward flow reaches a maximum and then decreases with height. Sometimes this situation appears also in the north, but, as the sections illustrate, the slope reversal is often not clearcut and northward rising isanosteres are sometimes found near the naviface (Montgomery, 1969). Nevertheless, leveling and reversal above in the isanosteres is not uncommon. Thus there frequently are eastward flow maxima below the thermocline in the Northern Hemisphere. When such eastward flows have significant extension at their latitudes they may be called countercurrents in the sense usually understood. To the extent that a velocity maximum exists below the thermocline, they can be characterized as subsurface or, more accurately, subthermocline countercurrents.[1]

Between the outer sides of the W-shaped isanosteres is a region of small vertical gradient (Figs. 1a and 1b), the equatorial thermostad. It corresponds to what Montgomery and Stroup (1962) call the 13-C water in the equatorial Pacific. The modal temperature of the layer in the Atlantic is about 13°C, but the temperature is a little higher during northern summer than during winter in the western part of the ocean (Cochrane, 1975). As Figs. 1a and 1b suggest, much of the transport of subsurface countercurrents is in the thermostad.

3. The subthermocline countercurrents at 140 cl t^{-1}

The surface where δ_T = 140 cl t^{-1} lies within the upper part of the thermostad across the equatorial Atlantic Ocean during the entire year (Cochrane, 1968b). It is analogous to the 160 cl t^{-1} surface in the less saline Pacific which Tsuchiya (1968, 1972, 1975) used in studying the subsurface countercurrents of that ocean. Fig. 2a, from Kelly's (1978) study of currents and waters at 140 cl t^{-1}, shows the distribution of acceleration potential relative to 800 db based on data from February, March and April (FMA); Fig. 2b shows the distribution for July, August and September (JAS) data. The depth of the surface ranges from 100 to 300 m, approximately, during both periods. Data from 1963 (Equalant I) and 1968 (*Crawford*) form the basis for Fig. 2a and data from 1963 (Equalant II), 1964 (*Alaminos*) and 1974 (GATE) that for Fig. 2b. Where data overlap in the latter map, preference has been given to the 1964 data because of its greater coverage. Significant differences among years exist (Cochrane, 1975), but the same major features are found in all cruises. Minor features from individual years are smoothed. Gradients must be viewed with some caution because of the smoothing.

[1] The analysis, which is presented below, of the horizontal distribution of geostrophic flow somewhat below the thermocline suggests that the eastward component indicated in the Southern Hemisphere by the section in Fig. 1b is not a part of the subsurface countercurrent although its form is similar to a section across that current (see Fig. 2b).

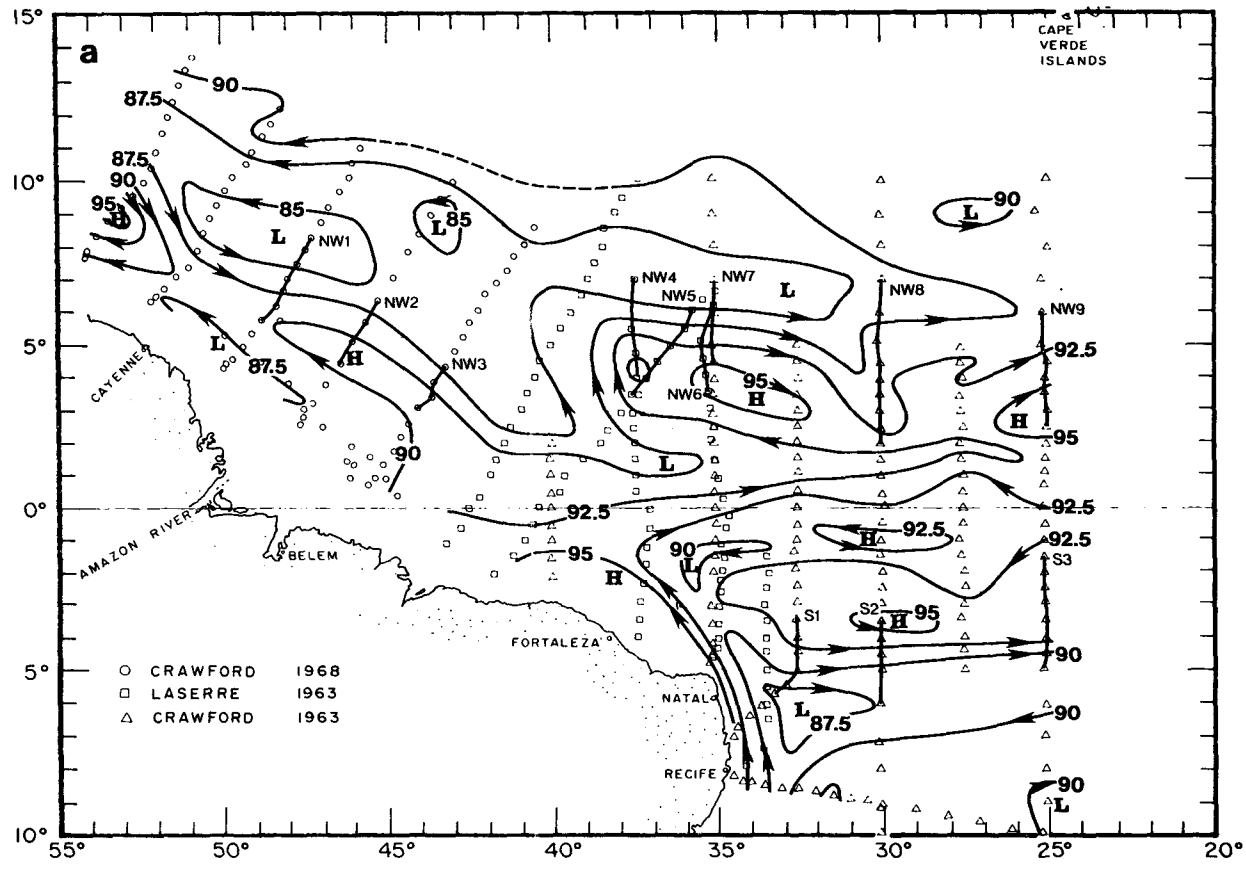

FIG. 2a. Acceleration potential (dyn cm) at 140 cl t^{-1} relative to 800 db for February–April data. Locations of some transects used in Tables 3 and 4 are shown.

a. Countercurrent Ridges and Troughs

At 140 cl t^{-1} in either hemisphere, an eastward flow, the countercurrent, lies between a zonally elongated ridge and similarly elongated trough, the Countercurrent Ridge and Trough. In both hemispheres the ridge is centered near a latitude of 3°. The ridges correspond to the deep portions of the W-shaped isosteres of Fig. 1. They are separated from the ridge or line of highs along the Equator, clearly in JAS, but to a smaller degree in FMA. The Countercurrent Troughs are centered near 7.5°S and 9°N. East of about 35°W, the northern trough and, at a corresponding distance from the African coast, the southern trough, have small poleward trends. Analogous ridges and troughs are of course present in the Pacific Ocean at 160 cl t^{-1}, as Tsuchiya (1968) and Love (1972) show. In the western Pacific, however, the ridges merge with the highs at the Equator so that the subsurface countercurrents are not distinct from the Undercurrent, as they are in the western Atlantic. The troughs are centered near 6°N and 6°S in the eastern Pacific (Tsuchiya, 1975), thus nearer the Equator than in the Atlantic.

The North Countercurrent Ridge begins in the west with an anticyclone or high, centered near 3.5°N, 47°W off the mouths of the Amazon River. It is found in all cruises covering the region: during FMA of 1963 and 1968 and during JAS of 1963, 1964 and 1973 (Brazilian Navy, 1975), although weaker during FMA. Because of its apparent permanence the feature is given a name, the Amazon Anticyclone. During JAS (Fig. 2b), it appears to have a considerable internal circulation. Anticyclones are encountered farther north and west than the Amazon Anticyclone, but they are usually weaker and more variable in position. Hence, the ridge is considered to begin with the Amazon Anticyclone.

East of the Amazon Anticyclone, the ridge is interrupted by a marked trough extending southeast from the main Countercurrent Trough centered near 7.5°N, 48°W. The interrupting trough is also found in all data covering the region, for FMA of 1963 and 1968 (different portions of the feature were covered in these years) and JAS of 1963, 1964 and 1973; the feature is suggested, but not established, by the GATE 1974 data which do not fully cover its region.

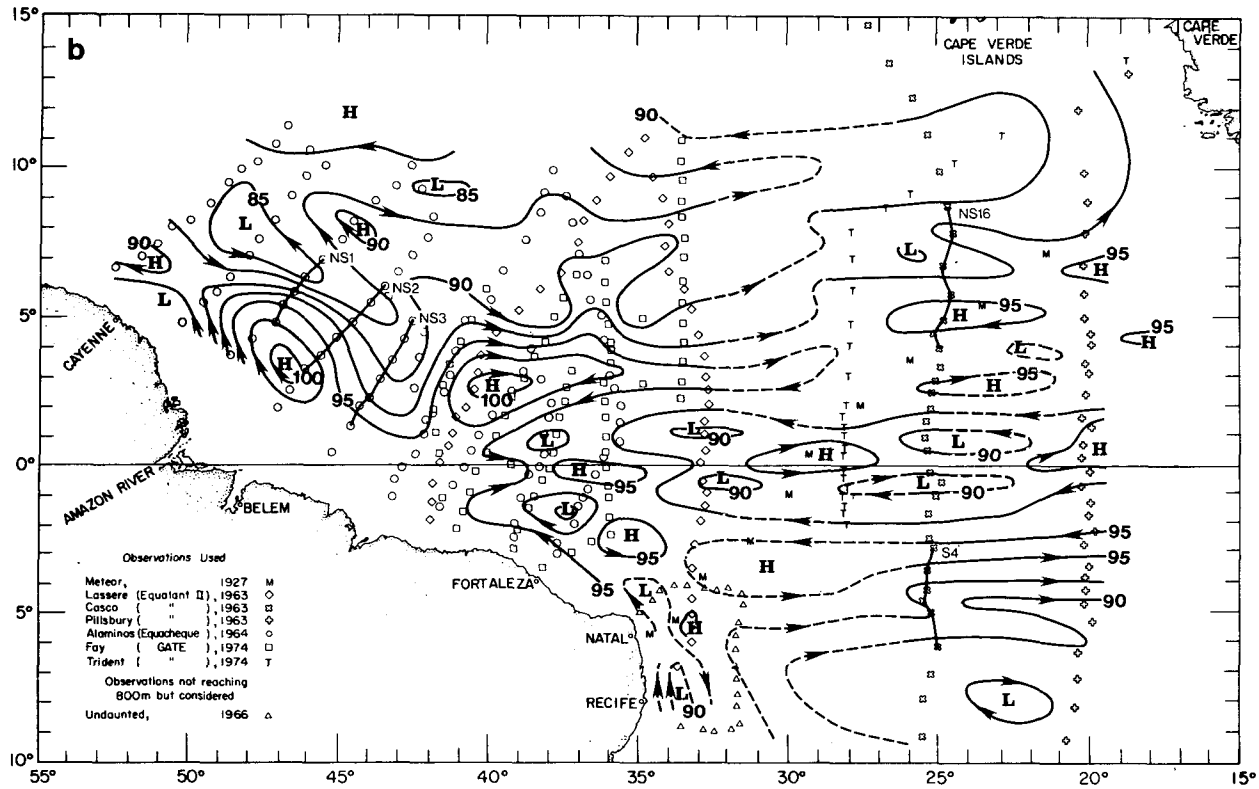

FIG. 2b. As in Fig. 2a except for July–September data. Locations for some transects used in Tables 1, 2, 3 and 4 are shown. Dashed contours indicate that available data do not provide a basis for a definitive analysis.

East of the trough, the Countercurrent Ridge is again present from 40°N to 30°W as a high, or a number of highs, centered along 3°N, approximately. The ridge has been encountered in that sector on all available cruises taken in FMA (1963) and in JAS (1963, 1964, 1973, 1974, and 1976). Considerable internal circulation is indicated by all cruises covering the region during either quarter. The eastern portion of the ridge (or series of anticyclones) appears to weaken in the *Crawford* lines of FMA at 27.5 and 30°W. The eastern portion is not clearly delineated by data for JAS, although by 25°W, the ridge has weakened as is noted below.

Along the north side of the ridge from 40 to 30°W, there are a number of secondary high regions during JAS and, to a lesser degree, during FMA. They, of course, indicate bands of eastward flow on their northern limbs. Such flow is small in comparison with that closer to the Equator near the main Countercurrent Ridge, but complicates the definition of the countercurrent. The eastern North Pacific ridge does not exhibit this complication so strongly as the Atlantic ridge perhaps because the Countercurrent Trough is at a somewhat lower latitude than in the North Atlantic.

From ~28°W east, the northern ridge weakens and one or two additional zonal ridges appear farther north. The north countercurrent evidently splits into a number of eastward bands, each considerably weaker than the single eastward flow farther west. Although the primary basis for such a structure in the map for JAS (Fig. 2b) is the *Casco* line at 25°W, there is considerably more evidence: the *Trident* lines at 28°W during GATE (Miller *et al.*, 1975) show a series of rises and falls in the isotherms rather than the single trough and rise of the north half of the W structure illustrated in Fig. 1. Merle's (personal communication, 1977) mean isotherms at 23.5°W for all GATE observational periods also indicate a northward rise in isotherms (below ~15°C) occurring north of 5°N, rather than north of 2 or 3°N as farther west (e.g., Fig. 1). The map for FMA (Fig. 2a) does not extend far to the east, but the breaking up seems to appear at 30°W; the *Zvezda* section at 20°W (Equalant I) shows a number of rises and falls in the isopycnals (σ_t) between 2 and 6°N (Kolesnikov, 1973).

The South Countercurrent Ridge appears to have a similar disintegrative structure in the east at comparable distances from the African coast. The vertical sections in the east (Kolesnikov, 1973) show the wider, multiple trough-ridge structures. Merle (1978) shows (mean annual σ_t at 300 m) that the ridge broadens east of ~30°W.

East of 100°W, roughly, in the Pacific, both Countercurrent Ridges break up into a series of more or less zonal ridges (Tsuchiya, 1975) as in the Atlantic. The distance from the onset of this feature to the eastern boundary is similar to that in the Atlantic.

In view of the form of the North Countercurrent Ridge, it is convenient for subsequent discussions to divide the subthermocline countercurrent into three sectors, that of the "Amazon Anticyclone" from 50 to 40°W, approximately, the "main" sector north of the highs between 40 and 28°W, approximately, and a "disintegrative" sector farther east.

b. *Relationships to coastal currents and the Undercurrent*

At 140 cl t^{-1} all of the eastward flows near the Equator can be traced back in part to currents along the Brazilian coast: the northward flow along the east coast from 10°S, or farther south, to Cape Saõ Roque, and the westward flow along the north coast (or shelf break), the North Brazilian Current [Metcalf and Stalcup (1967) use the name North Brazilian Coastal Current].

The origin of the south countercurrent is delineated rather clearly by the acceleration potential for FMA (Fig. 2a). Eastward flow first appears near 3°S, 35°W, where the northward coastal current meets the southwestward flow from the north side of the South Countercurrent Ridge. A considerable part of the countercurrent farther east is formed by the circulation internal to the ridge. The origin, as shown for JAS in Fig. 2b, is complicated by the presence of two bands of northward flow, one immediately adjacent to the coast and the other separated from the first by a low. [The two bands are suggested by 1966 data from the *Undaunted*, reported by Goulet and Ingham (1971). The stations, however, did not reach 800 m.] Both bands appear to contribute to the South Countercurrent.

The Undercurrent appears in both maps. In JAS there is a series of highs along the Equator; in FMA a low lies at the Equator, although there are extensive bands of eastward flow north and south of the Equator. The Undercurrent at 140 cl t^{-1} apparently is stronger in JAS than in FMA.

As Metcalf *et al.* (1962) and others have noted, the coastal current (or currents) is the source of the water characteristics of the thermocline layers of the Undercurrent. Cochrane (1968b, 1975) and Kelly (1978) have noted that the Undercurrent also receives water into its subthermocline layers from the coastal current, as Figs. 2a and 2b indicate. Near 38°W a retroverse branch from the North Brazilian Current turns north along the west side of a low centered at ~1.5°S in the sector 38–36°W and then east to run into the Undercurrent. The low is indicated in both the *Laserre* and *Crawford* lines along 35°W in FMA 1963 and in the *Alaminos* 1964 and *Fay* 1974 observations during JAS.

At the west side of the Amazon Anticyclone near 50°W, a large part of the North Brazilian Current turns back toward the east. This eastward flow constitutes the beginning of the north countercurrent according to the definition used in this paper. The flow in the eastern limb of the Amazon Anticyclone heads largely to the southeast. Part of the flow reaches the Equator between 45 and 40°W where it joins the Equatorial Undercurrent. Such a path into the Undercurrent is suggested by the drogue paths and characteristic distributions which Metcalf and Stalcup (1967) encountered in 1965. Much of the flow in the eastern limb does not reach the Equator; instead it turns northward somewhere between 40 and 42°W and then eastward to constitute a large part of the north subthermocline countercurrent. The sources of the latter and the Undercurrent are thus intimately intertwined.

4. Geostrophic velocity and transport

a. *Fay transect at* 33.5°W

As Figs. 1a and 1b illustrate, the subthermocline eastward flow between 3 and 9°N, in contrast to its analogue in the Southern Hemisphere, is not distinctly separated from the flow in the navifacial layers. In order to develop a definition of a *subthermocline* countercurrent which applies in either hemisphere, a transect in the less simple Northern Hemisphere is examined in detail. Fig. 3 shows the cross section of thermosteric anomaly for the transect made by the R/V *Fay* at 33.5°N during August 1974. Geostrophic velocities normal to the transect (relative to 800 db) were computed for each adjacent station pair at 10 cl t^{-1} intervals from 80 to 200 cl t^{-1} and at 20 cl t^{-1} intervals above 200 cl t^{-1}. Table 1 gives the velocities (at 20 cl t^{-1} intervals) and Table 2 the corresponding transports. The example is fairly typical, although more complex than average.

Despite the complexities in the transect, the velocity maxima and preponderance of transport below the base of the thermocline (below 200 cl t^{-1}) seem to justify the name *subthermocline* countercurrent for much of the flow. In order to exclude the eastward flow above the thermocline in the Northern Hemisphere, the upper boundary of the current is taken at 200 cl t^{-1}, a value which is also suitable for the Southern Hemisphere. The lower boundary is taken at 80 cl t^{-1} where, in both hemispheres, the baroclinicity is small. The current must lie between the Countercurrent Ridge and Trough. (The condition is applied at 140 cl t^{-1}.) Since, as already noted, there are secondary highs north of the Northern Countercurrent Ridge, the current is considered to lie between the two stations along a transect for

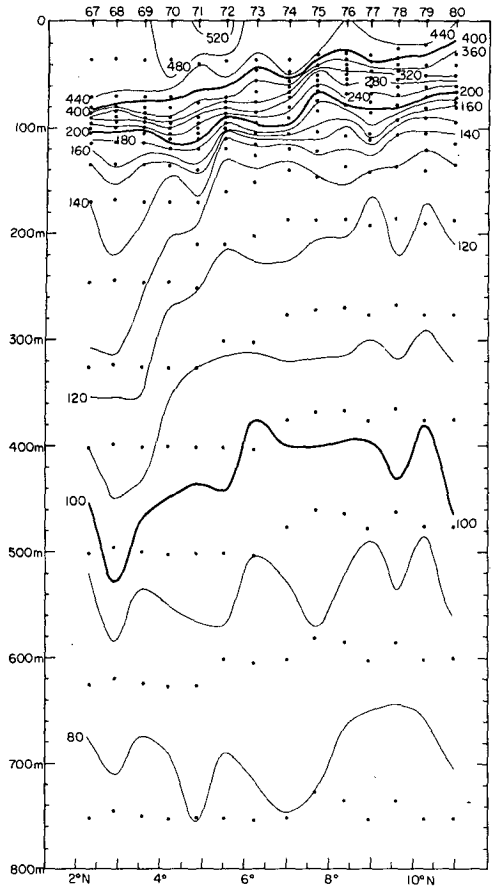

FIG. 3. Vertical section of thermosteric anomaly (cl t^{-1}) at 33.5°W from the *Fay* cruise of GATE (18–20 August 1974). Vertical exaggeration 2.76 × 10^3:1. Station positions are given at top. Location is shown in Fig. 4.

which the net eastward transport is found to be largest.

In the transect, the definition implies that the current is present between stations 68 and 77, and includes not only the large eastward flow between stations 68 and 70, but also the secondary eastward and intervening westward flows farther north. Accordingly, the current has a total geostrophic transport of nearly 21 × 10^6 m^3 s^{-1}. A large part of the transport, 77%, is found in the layer from 100 to 140 cl t^{-1}.

If the navifacial countercurrent is defined as the flow *above* 200 cl t^{-1} between stations which maximize the eastward transport, it lies between stations 68 and 79, thus extending farther north than the subthermocline countercurrent.

b. Results for available transects

Geostrophic velocities and transports for all available transects across the north and south subthermocline countercurrent at 25°W or farther west were computed in the same manner as that used in the example above. Table 3 lists important aspects of the computed results for the south countercurrent and Table 4 those for the north countercurrent. The locations of the transects are shown in Figs. 2a, 2b and 4. Although some of the transects probably do not cross the entire countercurrent as defined above, they are included because they cross the principal band of eastward flow, which, as the example indicates, accounts for much of the total transport. Because of this, the meridional width of the current given in the tables is that of the principal eastward flow *uninterrupted* by any net westward flow in the 80–200 cl t^{-1} layer.

c. South subthermocline countercurrent

The core of the simpler countercurrent in the Southern Hemisphere may be considered to be at about 138 cl t^{-1}, the mean thermosteric anomaly at the velocity maximum for all adjacent station pairs

TABLE 1. Geostrophic velocity (cm s^{-1}) component normal to transect for *Fay* 1974 stations 68–79 at 33.5°W. Positive values have an eastward component.

δ_T (cl t^{-1})	Stations										
	68	69	70	71	72	73	74	75	76	77	78	79
Naviface	45	5	29	53	43	−15	45	9	−4	−4		16
480			38	50								
440	43	19	27	53	30	−13	45			−6		16
400	41	18	22	53	23	−9	39	−2	2	−6		16
360	42	17	17	52	16	−7	34	−4	4	−6		15
320	46	19	10	50	11	−7	28	−4	5	−5		16
280	50	21	5	47	9	−7	20	−1	4	−5		15
240	51	25	−1	44	7	−7	13	3	3	−4		14
200	51	31	−5	37	7	−6	4	6	3	−4		13
180	51	34	−6	33	8	−6	0	7	4	−4		12
160	49	36	−5	27	9	−6	−3	8	6	−6		10
140	41	33	−2	19	10	−6	−3	7	8	−8		10
120	29	15	−3	8	12	−7	−2	7	6	−8		8
100	21	−5	−10	5	9	−5	−3	7	4	−4		3
80	3	−3	−4	2	−1	−1	0	3	1	0		0

TABLE 2. Geostrophic transport (10^6 m^3 s^{-1}) for the *Fay* transect at 33.5°W. The upper rectangle encloses the north navifacial countercurrent; the lower rectangle, the north subthermocline countercurrent. Positive values have an eastward component.

	Stations												
δ_T (cl t^{-1})	68	69	70	71	72	73	74	75	76	77	78	79	
480-naviface			0.93[1]	0.98[1]								1.96	Transect totals[2]
440-480	2.20[1]	0.58[1]	0.23	0.80	1.18[1]	-0.52[1]	1.32[1]			-0.06[1]	0.23[1]	5.96	
400-440	0.36	0.13	0.31	0.68	0.23	-0.09	0.15	0.08[1]	-0.03[1]	-0.07	0.13	1.88	
360-400	0.20	0.15	0.16	0.36	0.16	-0.05	0.13	-0.02	0.01	-0.03	0.13	1.20	
320-360	0.15	0.08	0.07	0.27	0.09	-0.05	0.12	-0.02	0.02	-0.02	0.08	0.79	
280-320	0.26	0.07	0.03	0.20	0.06	-0.04	0.09	-0.01	0.03	-0.03	0.07	0.73	
240-280	0.18	0.09	0.01	0.24	0.03	-0.05	0.15	0.01	0.03	-0.04	0.12	0.77	Transect total[3]
200-240	0.20	0.12	-0.03	0.29	0.05	-0.09	0.07	0.03	0.02	-0.04	0.08	0.70	13.99
180-200	0.38	0.19	-0.03	0.16	0.03	-0.02	0.01	0.03	0.02	-0.03	0.04	0.77	Transect totals[2]
160-180	0.70	0.21	-0.04	0.24	0.04	-0.02	-0.01	0.08	0.04	-0.03	0.05	1.24	
140-160	2.49	0.97	-0.07	0.34	0.06	-0.05	-0.04	0.16	0.12	-0.09	0.12	3.98	
120-140	4.07	2.48	-0.17	0.85	0.92	-0.65	-0.15	0.41	0.31	-0.48	0.58	8.07	
100-120	3.00	0.50	-0.88	0.85	1.61	-0.91	-0.39	1.00	0.65	-0.94	0.83	5.43	
80-100	1.49	-0.66	-1.59	0.98	0.59	-0.90	-0.30	1.19	0.40	-0.33	0.16	1.20	
800 db- 80	0.14	-0.11	-0.10	0.07	-0.03	-0.03	0.01	0.10	0.03	-0.03	-0.03		Transect total[4]
Total[4]	12.13	3.69	-2.78	3.42	3.25	-2.55	-0.88	2.87	1.54				20.69

[1] Transport between first δ_T listed and naviface.

[2] For stations 68 to 79 for δ_T above 200 cl t^{-1} and for stations 68 to 77 below 200 cl t^{-1}.

[3] For layer down to 200 cl t^{-1}.

[4] For 80-200 cl t^{-1} layer.

TABLE 3. Geostrophic calculations for the subthermocline countercurrents, Southern Hemisphere.

Ship	Stations	Date (GMT)	Lat.	Long. (W)	Transect[1]	Width[2] (km)	Highest velocity (cm s^{-1})[3]	δ_T at highest velocity	Lat. at highest velocity[4]	Highest navifacial velocity[5] (cm s^{-1})	Transport ($10^6 m^3 s^{-1}$) for δ_T intervals[6] 80	100	120	140	160	180	200	Total
Crawford	1438	21 III '63	6°03'	33°44'														
	1444	22 III '63	5°44'	33°19'	S1	247	29	130	4°43'	19	2.7	4.6	6.1	1.9	0.4	0.1		15.9
	1426	11 III '63	3°30'	30°06'														
	1430	13 III '63	6°02'	30°07'	S2	283	62	145	4°41'	54	2.7	5.2	8.5	2.9	0.4	0.4		20.1
	1353	10 II '63	1°35'	25°00'														
	1362	14 II '63	4°57'	25°10'	S3	165	62	140	4°15'	42	0.8	4.6	5.5	1.4	0.6	0.2		13.1
Casco	36	10 VIII '63	2°51'	25°04'														
	41	11 VIII '63	6°02'	24°58'	S4	142	31	200N	3°51'	98	0.9	2.4	4.9	3.5	0.7	0.6		13.0
	Means					209	46	138[7]	4°22'		1.8	4.2	6.2	2.4	0.5	0.4		15.4

[1] Shown in Fig. 2a, 2b, or 4.
[2] Uninterrupted meridional width.
[3] Component normal to transect and with eastward component in the layer from 80 to 200 cl t^{-1}.
[4] In 80 to 200 cl t^{-1} layer. M indicates a maximum at 200 cl t^{-1}. N indicates no maximum, but monotonic increase to vicinity of naviface.
[5] Component normal to transect and with eastward component.
[6] cl t^{-1}.
[7] Mean for subthermocline velocity maxima for all adjacent station pairs in transect.

(Table 3). The mean uninterrupted meridional width of the current is 209 km. The mean geostrophic transport is 15.4×10^6 m^3 s^{-1}. The largest proportion of the transport, 40%, is carried in the layer from 120 to 140 cl t^{-1}, which is in the thermostad and normally contains the velocity maximum.

It is perhaps noteworthy that, despite the prevalence of westward flow above 200 cl t^{-1}, every transect indicates some eastward geostrophic velocity at the naviface. Evidently, such eastward flow is largely masked by the prevailing wind drift since it does not appear in pilot chart information (e.g., Schumacher, 1940).

d. Core of the north subthermocline countercurrent

The geostrophic computations for the north countercurrent indicate that an eastward velocity maximum below 200 cl t^{-1} is present between at least one pair of adjacent stations in every transect. Usually the maximum is marked clearly and often it is higher than the highest eastward velocity at the naviface (Table 4). In the main sector, the mean thermosteric anomaly for all subthermocline maxima is 148 cl t^{-1}, 10 cl t^{-1} higher than the corresponding value for the south countercurrent. The velocity maxima in the Amazon Anticyclone and disintegrative sectors are less clearly marked.

The frequent presence of eastward flow above the north subthermocline countercurrent casts some doubt on the suitability of the definition of the current. However, justification beyond that discussed up to this point is provided by comparing the cores of eastward flow between the naviface and the 140 cl t^{-1} surface (between the navifacial and subthermocline core layers). Fig. 5 shows the geopotential at the naviface for JAS superposed on the acceleration potential at 140 cl t^{-1} from Fig. 2b; both fields are based on the same stations. Most of the highs for the two surfaces do not coincide and the paths of the current cores coincide in only a few locations. A similar lack of connection is apparent for FMA.

e. North subthermocline countercurrent

In the Amazon Anticyclone sector of the north subthermocline countercurrent (~50–40°W), the limited set of transects (Table 4) indicates a strong annual increase in transport from FMA to JAS. The cycle is similar to the well-established cycles in the navifacial velocities. The distributions of transport among isanosteric layers also exhibits an annual change with an increase of transport from FMA to JAS in the layers with higher thermosteric anomaly.

In the main sector (~40–28°W), the evidence for a permanent eastward transport below the thermocline (below 200 cl t^{-1}) is strong. All 17 transects from four years, from FMA and from JAS (Table 4), indicate substantial transports. The considerable range of transports suggests, along with the flow pattern at 140 cl t^{-1} (Figs. 2a and 2b), that the transects represent crossings of the eastward limbs of anticyclones of varying intensities and slopes. Significant change in transport sometimes occurs within rather short time intervals, as the *Gyre* transects NS12 and 13 illustrate. However, no available transect in the region fails to show strong eastward flow below 200 cl t^{-1}.

The mean transport in the main sector for FMA is only a little smaller than that for JAS; the difference is not statistically significant. Like the corresponding eastern Pacific current (Tsuchiya, 1975), the subthermocline flow exhibits marked independence from the overlying flow above the thermocline where both the transect data and pilot charts (e.g., Schumacher, 1940) show a large annual cycle. Thus the character of the subthermocline flow appears to change in the rather short distance between the Amazon Anticyclone sector and main sector from one with considerable annual variation to one with little or none.

The main sector of the north countercurrent does not differ greatly from the south countercurrent (Tables 3 and 4): the mean transport is not notably larger; the mean uninterrupted meridional widths are similar; the flux modes are in the same layer; and the mean latitudes of the current core are similar.

The disintegrative sector of the north countercurrent (east of ~28°W) is represented in Table 4 by only two transects. Although the *Crawford* transect for FMA is like the average for the main sector, the *Casco* transect for JAS has a markedly smaller transport than the average for the main sector, a shallower flux mode, and a higher latitude at the current core. As already noted, these and other aspects of the *Casco* transect are confirmed by other crossings.

f. Comparison of the Atlantic and Pacific subthermocline countercurrents

Although similarities among the subthermocline countercurrents of both the Atlantic and Pacific Oceans are extensive, the countercurrent of the North Atlantic has important peculiarities. The Amazon Anticyclone sector has an annual variation in strength. The North Countercurrent Trough is at higher latitude. Important secondary bands of eastward flow are often encountered north of the principal core of the countercurrent. The separation of the subthermocline flow from that above is less complete. The main sector is shorter than the correspondingly marked segments of the Pacific countercurrents.

TABLE 4. As in Table 3 except for the Northern Hemisphere.

Ship	Stations	Date (GMT)	Lat.	Long. (W)	Transect[1]	Width[2] (km)	Highest velocity (cm s^{-1})[3]	δ_T at highest velocity[4]	Lat. at highest velocity	Highest navifacial velocity[5] (cm s^{-1})	Transport ($10^6 m^3 s^{-1}$) for δ_T intervals[6] 80	100	120	140	160	180	200	Total
								Amazon-Anticyclone Sector, Feb.-Mar.- Apr.											
Crawford	2435	14 II '68	8°18'	47°16'														
	2441	15 II '68	5°44'	45°48'	NW1	285	52	200N	6°19'	116	0.9	1.2	0.7	0.5	0.6	0.7		4.6
	2451	18 II '68	4°24'	46°26'														
	2454	19 II '68	4°19'	45°15'	NW2	216	36	200N	6°01'	71	2.3	2.4	1.4	0.6	0.5	0.6		7.8
	2471	24 II '68	6°21'	41°56'														
	2474	25 II '68	3°03'	44°04'	NW3	141	88	200M	4°04'	78	3.4	4.9	3.3	1.3	1.3	1.3		15.5
	Means					214	59				2.2	2.8	1.8	0.8	0.8	0.9		9.3
								Amazon-Anticyclone Sector, Jul.-Aug.-Sep.											
Alaminos	94	3 IX '64	6°28'	45°54'														
	97	4 IX '64	4°48'	47°07'	NS1	185	83	200N	5°36'	71	4.5	5.9	6.7	3.8	1.5	0.6		23.0
	77	30 VIII '64	2°58'	46°16'														
	82	31 VIII '64	5°56'	43°30'	NS2	217	55	180	3°16'	65	4.2	6.4	6.5	6.4	2.6	2.0		28.0
	68	28 VIII '64	4°16'	42°43'														
	73	29 VIII '64	1°13'	44°40'	NS3	339	102	200M	2°35'	40	2.8	7.4	7.2	4.1	2.4	1.4		25.4
	Means					247	80				3.8	6.6	6.8	4.8	2.2	1.3		25.5
								Main Sector, Feb.-Mar.-Apr.											
Laserre	71	7 IV '63	4°01'	37°27'														
	74	8 IV '63	7°02'	37°30'	NW5	335	33	150	6°16'	26	2.3	2.8	4.2	5.2	1.2	0.5		16.2
	39	15 III '63	6°04'	35°44'														
	44	17 III '63	3°30'	37°37'	NW6	109	53	190	5°45'	38	3.5	4.5	3.4	1.4	0.4	0.3		13.5
	33	13 III '63	4°02'	35°20'														
	36	14 III '63	6°13'	35°06'	NW7	242	43	180	4°51'	29	3.5	4.5	6.5	3.6	1.5	0.7		20.5
Crawford	1465	28 III '63	6°59'	35°04'														
	1468	29 III '63	4°29'	35°05'	NW8	277	35	170	4°45'	18	1.5	3.0	4.5	2.5	0.6	0.6		12.7
	1407	6 III '63	7°00'	30°03'														
	1415	8 III '63	1°58'	30°05'	NW9	168	39	100	2°13'	57	6.0	8.9	9.0	3.3	0.6	0.4		28.2
	Means					226	41	150[7]	4°46'		3.4	4.7	5.5	3.2	0.9	0.5		18.2

								Main Sector, Jul.-Aug.-Sep.									
Fay	4	27 VII '74	5°00'	40°27'													
	6	28 VII '74	3°31'	41°08'	NS4	165	101	180	3°53'	57	6.1	4.4	7.3	16.7	4.5	0.9	39.9
Alaminos	14	29 VII '64	2°33'	41°29'													
	23	1 VIII '64	10°00'	37°40'	NS5	359	68	140	3°24'	64	3.3	6.1	7.0	4.4	0.6	0.6	22.0
Gyre	26	5 VII '76	6°35'	37°55'													
	30	6 VII '76	3°31'	39°42'	NS6	270	39	200N	5°23'	95	1.1	3.7	6.0	2.0	0.4	0.2	13.4
Fay	20	31 VII '74	2°24'	39°05'													
	23	31 VII '74	4°14'	38°00'	NS7	204	96	150	3°58'	43	3.5	7.4	9.4	11.6	2.1	0.5	34.5
Gyre	8	29 VI '76	3°30'	36°30'													
	13	30 VI '76	5°54'	36°36'	NS8	266	37	140	4°12'	82	1.1	3.7	6.7	2.6	0.5	0.3	14.9
	18	3 VII '76	3°00'	36°30'													
	22	3 VII '76	5°00'	36°14'	NS9	222	42	150	3°15'	30	0.8	3.6	8.4	2.2	0.3	0.4	15.7
Fay	56	14 VIII '74	2°14'	37°20'													
	60	16 VIII '74	5°02'	34°48'	NS10	312	27	200N	4°30'	70	4.4	5.9	5.1	2.5	0.7	0.5	19.1
Alaminos	23	1 VIII '64	10°00'	37°40'													
	30	2 VIII '64	4°14'	36°11'	NS11	162	42	200N	5°8'	49	2.0	4.0	6.5	2.8	1.0	0.6	16.9
Fay	29	1 VIII '74	5°35'	35°57'													
	32	3 VIII '74	3°31'	35°55'	NS12	232	39	200N	3°50'	89	1.3	3.6	3.8	2.9	0.5	0.6	12.7
	62	16 VIII '74	4°48'	35°54'													
	65	17 VIII '74	2°50'	36°08'	NS13	218	41	150	3°8'	36	2.5	5.2	6.7	2.4	0.5	0.2	17.5
	68	18 VIII '74	2°52'	33°29'													
	77	20 VIII '74	8°57'	33°31'	NS14	148	51	200M	3°13'	53	1.1	5.4	8.2	4.0	1.2	0.8	20.7
Laserre	25	13 VIII '63	7°26'	34°01'													
	28	14 VIII '63	5°15'	33°15'	NS15	243	36	180	5°38'	50	3.4	3.7	4.5	3.0	1.0	0.5	16.1
	Means					233	50	146[7]	4°7'		2.6	4.7	6.6	4.8	1.1	0.5	20.3
								Disintegrative Sector									
Crawford	1339	7 II '63	5°55'	25°11'													
	1345	8 II '63	2°29'	25°04'	NW10	270	28	170	4°40'	52	0.8	4.6	5.5	1.4	0.6	0.2	13.1
Casco	16	4 VIII '63	8°52'	24°37'													
	22	7 VIII '63	3°59'	24°56'	NS16	226	46	200	6°22'	95	(-1.0)	0.4	1.4	2.9	3.0	0.7	7.4[8]

[1] Shown in Fig. 2a, 2b, or 4.
[2] Uninterrupted meridional width.
[3] Component normal to transect and with eastward component in the layer from 80 to 200 cl t^{-1}.
[4] In 80 to 200 cl t^{-1} layer. M indicates a maximum at 200 cl t^{-1}. N indicates no maximum, but monotonic increase to vicinity of naviface.
[5] Component normal to transect and with eastward component.
[6] cl t^{-1}.
[7] Mean for subthermocline velocity maxima for all adjacent station pairs in transect.
[8] Between 100 and 200 cl t^{-1}.

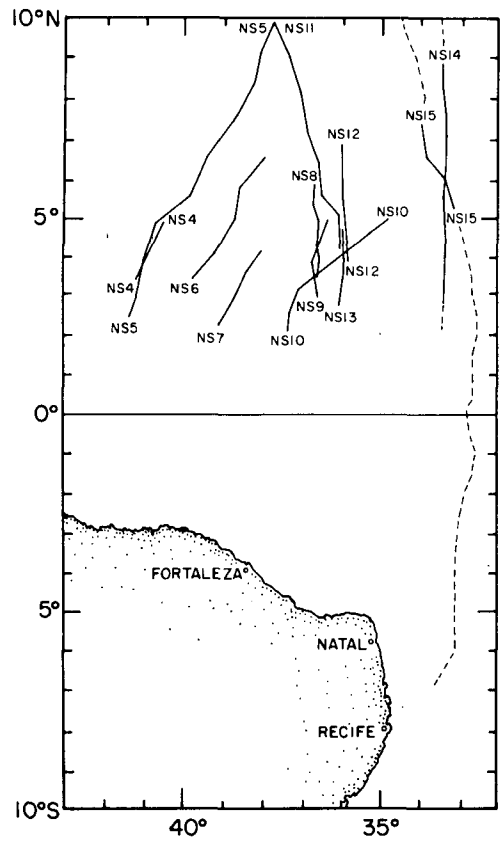

FIG. 4. Locations of transects in the main sector of the north subthermocline countercurrent. NS15 and dashed extensions show transect used in Fig. 1b. NS14 and dashed extensions show transect used in Fig. 3.

Because of some of the peculiarities, the definition of subthermocline countercurrent developed above is not as simple as the one Tsuchiya (1975) used for Pacific countercurrents; the latter includes all of the eastward flow above 500 db that lies between the stations at either end of the sharp slope of isanosteres, but not any secondary eastward flow. He computed geostrophic velocities between the station pair specified above, not between each adjacent station as in the present study.

The countercurrents in the Atlantic are wider than the corresponding flows in the Pacific: 209 (south) and 230 km (north, main sector) versus 160 and 150 km, respectively, in the Pacific. The widths given for the Atlantic (Tables 3 and 4) are uninterrupted widths and are thus comparable to those determined for the Pacific. Both countercurrents appear to be present to greater depths in the Atlantic: slight poleward rises can be detected in the isanosteres down to 800 m in the Atlantic, while Tsuchiya (1975) found that major slope of the isanosteres is limited to the upper 500 m in the Pacific.

Geostrophic transports for the two oceans may be compared only with caution because of the differing definitions used. Clearly, Tsuchiya's definitions and methods lead to smaller estimates of transport. However, the inclusion of secondary eastward flow in the Atlantic computations increases the transport usually by less than the approximate 25% found in the *Fay* transect discussed above (Table 2). Further, such augmenting of Atlantic transports is partly offset by the exclusion of transport above 200 cl t^{-1}. The difference in reference pressures seems to reflect actual difference in depth to which the Atlantic and Pacific currents extend. Accordingly, the Atlantic annual means, 15×10^6 (south) and 20×10^6 m^3 s^{-1} (north, main sector), represent considerably greater transports than Tsuchiya (1975) found in the eastern Pacific, 8×10^6 (north) and 4×10^6 m^3 s^{-1} (south).

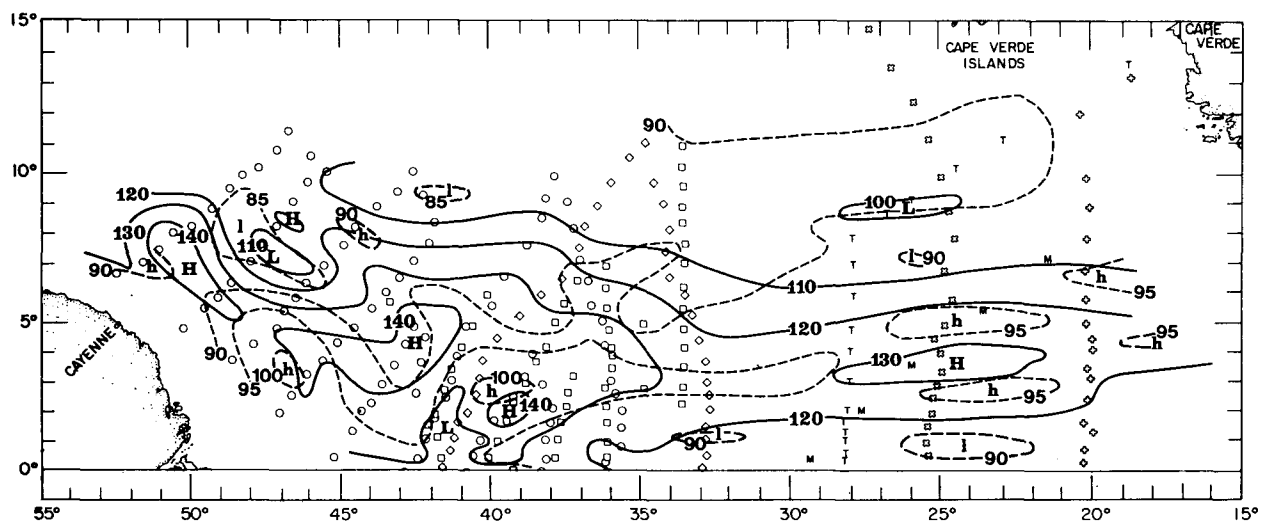

FIG. 5. Geopotential at naviface (full lines) superposed on acceleration potential at 140 cl t^{-1} (broken lines), both in units of dyn cm and both relative to 800 db for July–September. H and L show the centers of highs and lows at the naviface; h and l indicate the centers at 140 cl t^{-1}.

5. Summary

In each hemisphere of the equatorial Atlantic Ocean, the distribution of mass indicates a countercurrent (eastward flow) in the layers below the stronger portions of the thermocline (below a δ_T of 200 cl t^{-1}). The core is at roughly 4.5° from the Equator in either hemisphere, and near 140 cl t^{-1} in the south and near 150 cl t^{-1} in the north. The currents are present down to about 80 cl t^{-1} (nearly 800 m as Fig. 3 indicates).

The south subthermocline countercurrent, which appears to originate near 33.5°W, lies below predominantly westward flow in the navifacial and thermocline layers. (The region west of 25°W is investigated in the present paper.) Four transects indicate a mean uninterrupted width of 209 km and a mean geostrophic transport of 15×10^6 m^3 s^{-1} for the current (Table 3).

The north subthermocline countercurrent often lies below eastward flow in the navifacial and thermocline layers although its core and the path of its core are usually distinct from those of the overlying flow. As defined in this study, the countercurrent extends east from about 50°W through three sectors of differing structure and variation. From 50 to 40°W, approximately (the Amazon Anticyclone sector), the current, varying with the upper layers, is stronger in JAS than in FMA, according to available data (Table 4), and its core is rather poorly marked. From 40 to 28°W, approximately (the main sector), the evidence is strongest that the current is permanent: on all 17 available transects, from four years and from both FMA and JAS (Table 4), substantial eastward transport has been encountered in the layer from 80 to 200 cl t^{-1}. In this sector the mean uninterrupted width of the current is 231 km; the mean transport of the current in FMA is 18×10^6 m^3 s^{-1} and in JAS 20×10^6 m^3 s^{-1}; the difference in the means is not statistically significant. East of 28°W (disintegrative sector), the eastward flow is weaker and, apparently, breaks into a number of filaments.

Both the north and south subthermocline countercurrents are supplied in part from currents along the Brazilian coast. However, much of the transport of both countercurrents appears to be internal to the anticyclones on their equatorward flanks.

The transports in both of the Atlantic subthermocline countercurrents (west of 25°W) are, according to available data, considerably larger than those of their eastern Pacific counterparts.

Acknowledgments. Much of the research and the crucially important observations from *Laserre* (1963), *Alaminos* (1964), *Fay* (1974) and *Gyre* (1976) were supported by the Office of Naval Research, under Contract Nonr 2119[04] and the National Science Foundation, under Grant OCE74-11516 A 03.

REFERENCES

Bjerknes, V. and different collaborators, 1910: *Dynamic Meteorology and Hydrography*. Carnegie Institution, Publ. 88, 146 pp.

Brazilian Navy, 1975: *Atlas Oceanografico, Costa norte do Brasil*. Condicoes em Julho-Agosto 1973.

Cochrane, J. D., 1963: Equatorial Undercurrent and related currents off Brazil in March and April 1963. *Science*, **142**, 669–671.

——, 1965: Equatorial currents of the western Atlantic. Dept. of Oceanogr. Prog. Rep. Ref. 65-T, Texas A&M University, pp. 6–19 and 27.

——, 1968a: The equatorial thermostad in the western Atlantic Ocean. *Trans. Amer. Geophy. Union*, **49**, 199–200.

——, 1968b: The currents and waters in the western Tropical Atlantic Ocean. Dept. of Oceanogr. Prog. Rep. Ref. 68-8T, Texas A&M University, pp. 21–25 and Figs. 5, 6, 7.

——, 1975. Portions of a proposal for research on the North Equatorial Countercurrent System of the Atlantic Ocean west of 25°W. Dept. of Oceanogr. Prog. Rep. Ref. 75-7T, Texas A&M University, 112 pp.

Goulet, J. R., Jr., and M. C. Ingham, 1971: The shallow layer of high salinity in the southwestern tropical Atlantic Ocean. *Bull. Mar. Sci.*, **21**, 716–732.

Hisard, P., J. Citeau and A. Morliere, 1976: Le systeme des Contrecourants equatoriaux subsuperficiels, permanence et extension de la branche sud dans l'Ocean Altantique. *Cah. ORSTOM, Ser. Oceanogr.*, **14**, 209–220.

Kelly, F. J., 1978: Currents and waters at 140 cl t^{-1} in the western equatorial Atlantic during February–March–April. M.Sc. thesis, Texas A&M University, 59 pp.

Khanaychenko, N. K., 1970: Confirmation of the existence of the south branch of the equatorial countercurrent in the Atlantic Ocean. *Dokl. USSR Acad. Sci., Earth Sci Sec.* (Eng. translation), **187**, 235–236.

——, and N. Z. Khlystov, 1966: The south branch of the equatorial countercurrent in the Atlantic Ocean. *Dokl. USSR Acad. Sci.*, **166**, 205–207.

Kolesnikov, A. G., Ed., 1973: *Equalant I and Equalant II Oceanographic Atlas, Physical Oceanography*, Vol. 1. UNESCO, Paris: 289 pp. + pamphlet.

Love, C. M., Ed., 1972: *EASTROPAC Atlas*, Vol. 1. Circ. 330 Nat. Mar. Fish. Service, Washington, DC.

Mazeika, P. A., 1968: Eastward flow within the South Equatorial Current in the eastern South Atlantic. *J. Geophys. Res.*, **73**, 5819–5828.

Merle, J., 1978: Atlas hydrographique saisonnier de l'Ocean Atlantique intertropical. *Trav. Doc. ORSTROM*, **82**, 17 pp. + maps.

Metcalf, W. G., A. D. Voorhis, and M. C. Stalcup, 1962: The Atlantic Equatorial Undercurrent. *J. Geophys. Res.*, **67**, 2499–2508.

——, and M. C. Stalcup, 1967: Origin of the Atlantic Equatorial Undercurrent. *J. Geophys. Res.*, **72**, 4959–4975.

Miller, L., R. H. Weisberg and J. A. Knauss, 1975: Hydrographic observations during the GARP Atlantic Tropical Experiment (GATE): A preliminary report. Report, Grad. School Oceanogr., University Rhode Island, 197 pp.

Montgomery, R. B., 1937: A suggested method for representing gradient flow in isentropic surfaces. *Bull. Amer. Meteor. Soc.*, **18**, 210–212.

——, 1938: Circulation in the upper layers of the southern North Atlantic deduced with the use of isentropic analysis. *Pap. Phys. Oceanogr. Meteor.*, No. 6, 55 pp.

——, 1969: The words naviface and oxyty. *J. Mar. Res.*, **27**, 161–162.

——, and A. F. Spilhaus, 1941: Examples and outline of certain modifications in upper air analysis. *J. Aero. Sci.*, **9**, 276–283.

——, and E. D. Stroup, 1962: Equatorial waters and currents at 150°W in July–August 1952. *Johns Hopkins Oceanogr. Stud.*, **1**, 68 pp.

——, and W. S. Wooster, 1954: Thermosteric anomaly and the analysis of serial oceanographic data. *Deep-Sea Res.*, **2**, 63–70.

Reid, J. L., 1964: Evidence of a South Equatorial Countercurrent in the Atlantic Ocean in July 1963. *Nature*, **203**, 182.

——, 1965: Intermediate waters of the Pacific Ocean. *Johns Hopkins Oceanogr. Stud.*, **2**, 85 pp.

——, and R. J. Lynn, 1971: On the influence of Norwegian-Greenland and Weddell Seas upon the bottom waters of the Indian and Pacific Oceans. *Deep-Sea Res.*, **18**, 1063–1088.

Schumacher, A., 1940: Monatskarten der Oberflächenströmungen in Nordatlantischen Ozean (5°S bis 50°N). *Ann. Hydrogr. Mar. Meteor.*, **68**, 109–123.

Tsuchiya, M., 1968: Upper waters of the Intertropical Pacific Ocean. *Johns Hopkins Oceanogr. Stud.*, **4**, 55 pp.

——, 1972: A subsurface north equatorial countercurrent in the eastern Pacific Ocean. *J. Geophys. Res.*, **77**, 5981–5986.

——, 1975: Subsurface countercurrents in the eastern equatorial Pacific Ocean. *J. Mar. Res.* (Suppl.), **33**, 145–175.